In Vivo Glutamate Sensing inside the Mouse Brain with Perovskite Nickelate−Nafion Heterostructures

Yifei Sun,* Tran N. H. Nguyen, Adam Anderson, Xi Cheng, Thomas E. Gage, Jongcheon Lim, Zhan Zhang, Hua Zhou, Fanny Rodolakis, Zhen Zhang, Ilke Arslan, Shriram Ramanathan,* Hyowon Lee,* and Alexander A. Chubykin*

ACCESS | Metrics & More | Article Recommendations | SI Supporting Information

ABSTRACT: Glutamate, one of the main neurotransmitters in the brain, plays a critical role in communication between neurons, neuronal development, and various neurological disorders. Extracellular measurement of neurotransmitters such as glutamate in the brain is important for understanding these processes and developing a new generation of brain−machine interfaces. Here, we demonstrate the use of a perovskite nickelate−Nafion heterostructure as a promising glutamate sensor with a low detection limit of 16 nM and a response time of 1.2 s *via* amperometric sensing. We have designed and successfully tested novel perovskite nickelate−Nafion electrodes for recording of glutamate release *ex vivo* in electrically stimulated brain slices and *in vivo* from the primary visual cortex (V1) of awake mice exposed to visual stimuli. These results demonstrate the potential of perovskite nickelates as sensing media for brain−machine interfaces.
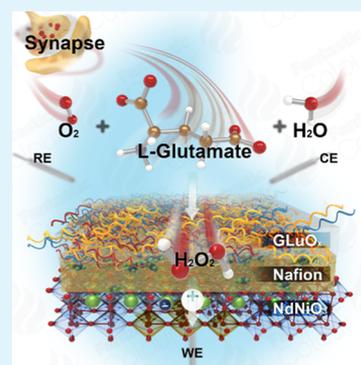
KEYWORDS: *glutamate, biosensor, nickelate, in vivo, strong correlated materials*

INTRODUCTION

Perovskite oxides (formula of ABO_3) are an important material family with a diverse range of physical properties and functionalities of interest to multiple disciplines in science and engineering. Among this class, rare-earth nickelates ($RNiO_3$ (RNO)), where R represents rare-earth lanthanide elements, have attracted significant interest in the fields of electronics, catalysis, and energy.[1−3] Perovskite nickelates are strongly correlated systems with electronic properties highly sensitive to the microstructure, strain, and defects.[4,5] The ground state at room or body temperature can be insulating or metallic depending on the steric effect due to the A-site cation, for instance, $NdNiO_3$ is a correlated metal at room temperature.[6−8] The highly tunable electronic properties of nickelates have served as motivation to exploit them as electrocatalysts in energy technologies[9] and biosensors.[10] There exists a great need for biosensing inside the brain tissue in living animals for *in vivo* measurements of neurotransmitters. Advancing *in vivo* techniques to monitor neurotransmitter release in the brain is of great interest and significance to neuroscience, disease therapy, and bioengineering fields, because these neurotransmitters play an essential role in critical brain functions such as information transmission, learning, and memory.[11−14] Furthermore, neurotransmission is known to be impaired in neurodegenerative disorders such as Parkinson's and Alzheimer's disease.[15] However, the precise measurements of neurotransmitters in the studies of these disorders are often lacking. Current technologies are being used to measure glutamate such as high-performance liquid chromatography, gas chromatography, mass spectrometry, and microdialysis. While these techniques result in a high level of accuracy, they require external analysis and longer measurement time.[16−18] On the other hand, genetically encoded glutamate sensors require genetic modification of the target cells. Thus, electrochemical sensors are well suited for *in vivo* measurements, in which direct and continuous measurements in the deep brain tissue can be carried out without the need for artificial labels or gene therapy.[19−22] Indeed, benchtop experiments exploring oxide electrodes for sensing of biomolecules have been reported.[23−25] However, multiple disciplines across natural sciences and engineering have to be brought together and numerous hurdles crossed to go from material-level sensing experiments to their use in implanted electrode devices for *in vivo* brain recording from live animals.

A particular neurotransmitter of interest is glutamate, which is among the most abundant and the main excitatory neurotransmitter in the central nervous system. It is involved
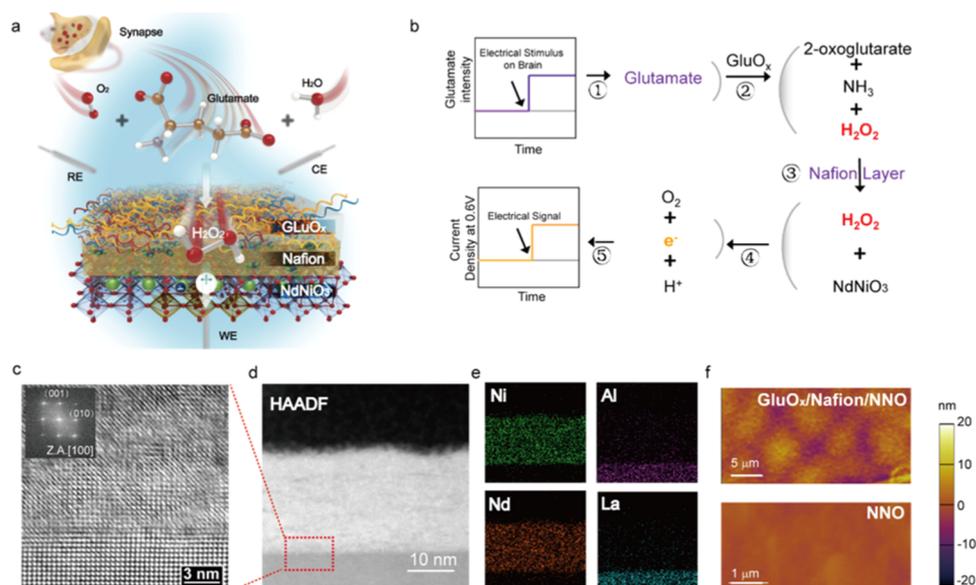
Figure 1. NdNiO$_3$/Nafion heterostructure as a glutamate biosensor. (a) Schematic of glutamate sensing with the nickelate–Nafion sensor. The NdNiO$_3$ (NNO) thin film was coated with Nafion followed by the GluO$_x$ enzyme. The Nafion serves as an ion-selective permeable membrane, while the GluO$_x$ enzyme is immobilized on the top of Nafion. (b) Biosensing reaction mechanism of glutamate by NNO. Electrical stimulus application led to the release of glutamate. The GluO$_x$ enzyme coated on NNO catalyzes the enzymatic reaction to form α-ketoglutarate, NH$_3$, and H$_2$O$_2$. The H$_2$O$_2$ diffuses through the Nafion to reach the surface of NNO. Under applied bias (*i.e.*, 0.6 V *vs* Ag/AgCl), the H$_2$O$_2$ oxidation is catalyzed by NNO, which is monitored by the electrochemical station. (c) High-resolution transmission electron microscopy (TEM) image of the NNO/LaAlO$_3$ (LAO) cross section. The fast Fourier transform (FFT) image of the interface is shown in the inset. (d) High-angle annular dark-field scanning TEM (HAADF-STEM) and (e) STEM-energy-dispersive X-ray (EDX) image of cross section of the NNO/LAO film. The selected area diffraction pattern is shown in the inset of (c). The epitaxially grown NNO film on the LAO substrate with uniformly dispersed Nd and Ni across the film thickness could be observed. (f) Surface morphology of GluO$_x$/Nafion/NNO and NNO characterized by atomic force microscopy (AFM). The surface of NNO is quite smooth. In comparison, the GluO$_x$ coating has a rough morphology of round-shaped particles with a diameter of ~5 μm, which is distinguishable from a bare NNO surface as well as the Nafion/NNO surface.

in many brain functions, including sensory perception, motor control, learning, memory formation, higher-level cognition, and behavior. As a result, changes in glutamate signaling or processing are involved in the pathophysiology of various neurological and neurodegenerative disorders.[26] Glutamate is highly excitatory and is rapidly removed from the synaptic cleft by transporters to prevent excitotoxic effects and excessive spillover to neighboring synapses.[27] Therefore, it is significant to understand how glutamatergic activity is regulated not only because much of the brain energy is spent on sustaining synaptic activity at the glutamatergic synapse but also due to glutamate's critical role in brain function at normal and disease-related levels.[28]

In a typical glutamate sensor fabrication process, glutamate oxidase (GluO$_x$) enzyme is immobilized on the surface of the sensing medium to trigger enzymatic generation of hydrogen peroxide (H$_2$O$_2$), which can be detected amperometrically.[29,30] To avoid the interference of other chemicals such as ascorbate, which can be directly oxidized on the electrode surface without an enzyme, a Nafion polymer layer is incorporated between the enzyme and sensing electrode. Nafion can electrostatically repel interference anions but selectively allows the penetration of H$_2$O$_2$. Such Nafion-coated structure has been reported to provide enhanced selectivity for accurate measurements.[31,32]

In recent years, several candidates for amperometric glutamate biosensors have been developed such as noble metals (*e.g.*, Pt, Au, and Pd[33,34]), glassy carbon, carbon fiber or carbon nanotubes (CNTs[35,36]), polymers,[37,38] binary metal oxides (*e.g.*, TiO$_2$ and CeO$_2$[39,40]), and perovskite oxides (*e.g.*, titanates).[23,41] Additionally, several studies have been

presented for implantation of glutamate sensors into the brain matter for real-time recording.[21,22,42,43] However, improving both response time scale and detection limit simultaneously motivates the discovery of new platforms for sensing. We report such a biosensor using a cross-linking immobilizing method with Nafion-coated perovskite nickelate thin films. Glutamate oxidase (GluO$_x$), an enzyme that metabolizes glutamate and releases H$_2$O$_2$, was immobilized on Nafion-coated NdNiO$_3$ (NNO) films. The as-generated H$_2$O$_2$ molecules penetrated through the Nafion and released protons and electrons catalyzed by NNO films. The released charge carriers were monitored using a three-electrode setup amperometrically. Here, for the first time, we present experimental demonstration of fast detection of low concentration (nanomolar range) of the glutamate in phosphate-buffered saline (PBS) using benchtop measurements, followed by *ex vivo* in mouse brain slices and *in vivo* in awake head-fixed mice using a correlated material system of perovskite nickelate (*i.e.*, NdNiO$_3$ (NNO)) heterostructured with Nafion, a polymeric ion-permeable membrane.

■ RESULTS

Figure 1a shows the schematic pathway for the glutamate sensing mechanism using NNO as a biosensor device. The electrical stimulus leads to an increased level of glutamate (path ① in Figure 1b), which gets transported to the device interface. The glutamate oxidase (GluO$_x$) enzyme is immobilized on the film surface, which consumes the glutamate with oxygen and water to produce H$_2$O$_2$. The GluO$_x$ biosensor is O$_2$-dependent, as suggested in eq 1 (path ②
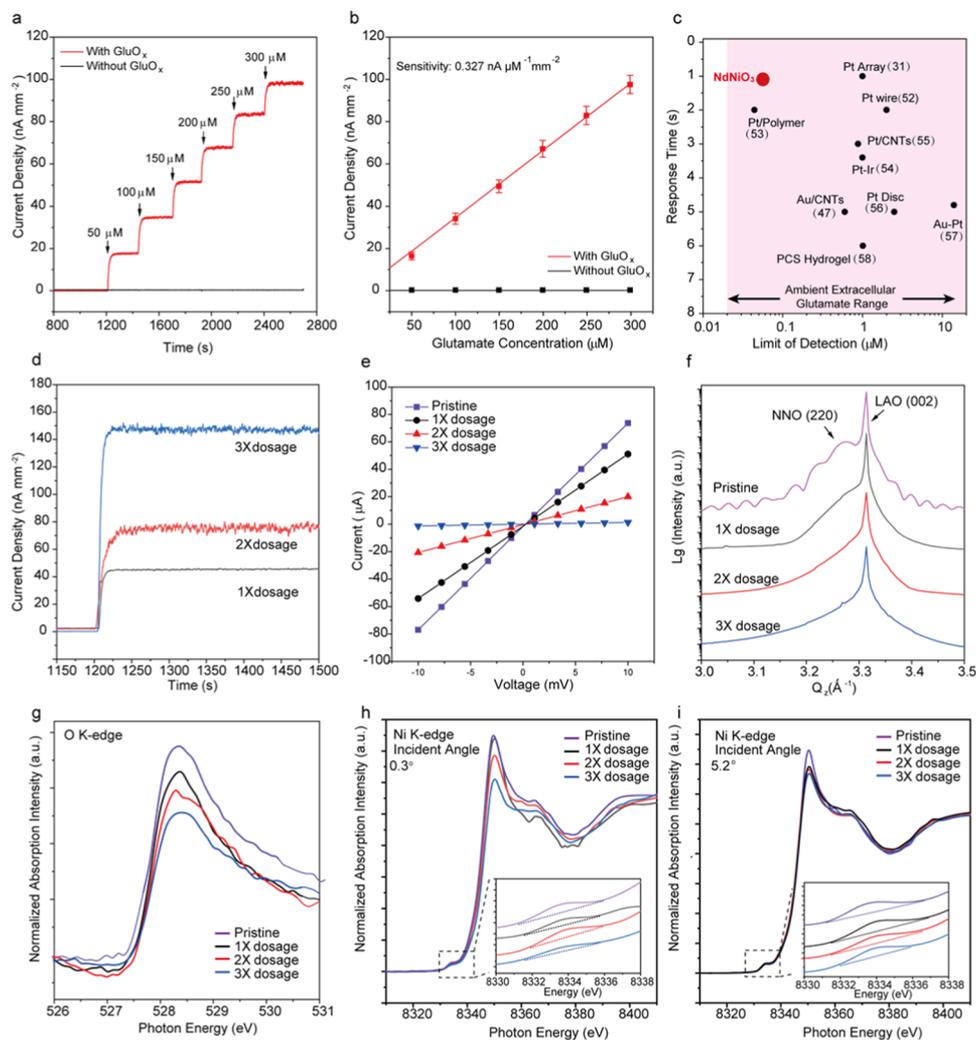
Figure 2. Benchtop experiments and nickelate characterization post-glutamate dosage. (a) Representative amperometric curves for NNO as a glutamate biosensor at the applied potential of 0.6 V *vs* Ag/AgCl in 0.01 M PBS (pH 7.4) with and without the presence of the GluO$_x$ enzyme (control). (b) Corresponding calibration curves and the sensitivity are shown. (c) Comparison of the performance metrics in terms of response time and detection limit of various representative glutamate biosensors from the literature. The light pink regime indicates the ambient extracellular glutamate level without any external stimulus. (d) Representative amperometric curves for NNO as a glutamate biosensor for different dosages of glutamate (100 μM per dosage) at an applied potential of 0.6 V *vs* Ag/AgCl in 0.01 M PBS (pH 7.4). (e) I−V curves taken from NNO films after treatment with 0× (pristine), 1×, 2×, and 3× dosages of glutamate. The evolution of resistivity of the films is shown in the inset. For instance, the 3× dosage treatment of glutamate led to the increase of the film resistivity by 2 orders of magnitude due to proton−electron incorporation. (f) Synchrotron X-ray diffraction (XRD) scans of identical NNO films upon the treatment of the pristine film and films subjected to 1×, 2×, and 3× dosages of glutamate. The scans are along the Q_z direction around the (002) diffraction peak of the LaAlO$_3$ (LAO) substrate (pseudocubic notation). (g) X-ray absorption curves of the O K-edge of NNO films after the treatment of 0× (pristine), 1×, 2×, and 3× dosages of glutamate. (h, i) Angle-dependent X-ray absorption spectra of the Ni K-edge of NNO films upon the treatment of 0× (pristine), 1×, 2×, and 3× dosages of glutamate at the incident angles of (h) 0.3° and (i) 5.2°. The zoom-in features of pre-edge area spectra are shown in the inset. The glutamate treatment leads to the gradually decreased intensity of the O K-edge absorption peak, pre-edge hump area, and white line intensity of Ni K-edge X-ray absorption near-edge spectroscopy (XANES), due to the intercalation of the proton and electron into the NNO lattice from the hydrogen peroxide oxidation.

in Figure 1b). However, it operates well in the brain under normal conditions without being limited by oxygen concentration[44]

$$\text{glutamate} + O_2 + H_2O$$
$$\rightarrow \alpha - \text{ketoglutarate} + NH_3 + H_2O_2 \quad\quad (1)$$
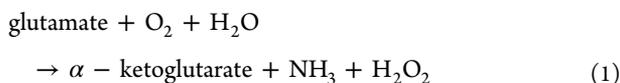
The H$_2$O$_2$ selectively penetrates through the Nafion film (path ③ in Figure 1b). H$_2$O$_2$ is then catalytically oxidized at the working electrode of NNO according to eq 2 (path ④ in

Figure 1b) at an appropriate polarization potential and monitored by the electrochemical station.

$$H_2O_2 \rightarrow O_2 + 2H^+ + 2e^- \quad\quad (2)$$

The protons intercalate into the nickelate lattice in which the proton is weakly bonded with oxygen anions and occupies interstitial sites in NiO$_6$ octahedra, and the extra electron is filled into the ligand hole in the Ni$_{3d}$−O$_{2p}$ hybridized orbital.[45,46] After the intercalation of the proton and electron, the electron−electron repulsion in the Ni site orbital leads to

the localization of electrons and an increase of resistivity, as a feedback mechanism.

The top-view and cross-section morphology of the NNO/LAO (NdNiO$_3$ thin film deposited on the LaAlO$_3$ substrate) film were analyzed by transmission electron microscopy (TEM). The interface between the NNO film and the LAO substrate is sharp without any secondary phases (Figure 1c,d). The NNO film is epitaxially oriented along the [001] direction, parallel to the c-axis of the LAO(001) substrate. The zone axis of the specimen is [100] for imaging and can be seen by the symmetry in the FFT image, as shown in the inset of Figure 1c. STEM-EDX analysis shown in Figure 1e illustrates the uniform distribution of Nd and Ni elements across the film thickness. The NNO film was coated with Nafion (a widely used ion-permeating membrane) and the GluO$_x$ enzyme. Atomic force microscopy (AFM) measurements were then performed to verify the surface decoration (Figures 1f and S3). The pristine NNO surface has a surface roughness of ~0.76 nm. In comparison, the first layer of Nafion coating leads to the increase of surface roughness to 8.54 nm (Table S1). Further GluO$_x$ coating shows up as a bright spot with a diameter of 5 μm.

Glutamate Biosensor Performance. The chronoamperometric method for the determination of glutamate utilizes the oxidation response of H$_2$O$_2$, a byproduct of enzymatic oxidation. From the cyclic voltametry (CV) scan results (representative result shown in Figure S4), 0.6 V vs Ag/AgCl is chosen as an optimal potential for amperometric detection of glutamate via oxidation of H$_2$O$_2$, which is also typically used in the literature.[20] Prior to sensing measurements, the NNO film was confirmed to have sufficient conductivity for reliable electrocatalytic activity (Figure S5). In the presence of oxygen, GluO$_x$ catalyzes successive reaction of glutamate to form H$_2$O$_2$, which can be oxidized at the electrode. As shown in Figure 2a, the perovskite nickelate film coated with Nafion−GluO$_x$ exhibits prominent electrocatalytic activity toward increasing levels of glutamate. The successive addition of glutamate (50 μM each dosage) leads to a significant jump up of current density of ~18 nA/mm^2 per dosage. In comparison, the nickelate without Nafion−GluO$_x$ demonstrates no current density variation upon addition of glutamate at 0.6 V vs Ag/AgCl, suggesting that there is no occurrence of Faradaic reaction (H$_2$O$_2$ → O$_2$ + H$^+$ + 2e$^-$) without the enzyme. A calibration plot is presented in Figure 1b, which presents a linear kinetic reaction with a sensitivity of 0.327 ± 0.07 nA/(μM mm^2) (n = 3) toward glutamate. For sensor selectivity, a Nafion layer, which electrostatically repels anions, was deposited onto the perovskite nickelate film before the immobilizing of the GluO$_x$ enzyme layer. Figure S6a shows the amperometric response of our glutamate biosensor against ascorbic acid (AA), uric acid (UA), and acetaminophen (AC). Figure S6b presents the current ratio between glutamate and AA, UA, and AC. There is very slight response from the sensor to UA and AC. The current ratio of AA/glutamate is 28% with a negligible ratio of UA/glutamate and AC/glutamate of 4 and 7%, respectively. The results suggested that the Nafion membrane can only prevent about 80% interference signal from AA. Therefore, in future studies, another type of a permselective layer such as m-phenylenediamine dihydrochloride can be applied to better block the interferent signal from AA and other species such as dopamine and 5-hydroxytryptamine.[47−51] One can also include a final layer of the ascorbate oxidase enzyme (200 U/mL) to further prevent the interference of AA.[47]

A comparison of the parameters for response time and limits of detection of various glutamate biosensors is shown in Figure 2c.[31,47,52−58] The light pink regime in Figure 2c represents ambient extracellular glutamate ranging from 20 nM to 20 μM.[21,59] The NNO film demonstrates a fast response time of ~1.2 s and a low detection limit of 16 nM with a linear range between 1 and 700 μM (Figure S7). These metrics are comparable to state-of-the-art glutamate sensors suggesting their potential as in vivo sensors as described further. Additionally, it is important for our glutamate sensor to maintain the balance between sensitivity, selectivity, and temporal resolution. Thus, the existence of the permselective membrane is also significant to keep our sensor selective, which increases the response time as comparing to the ultrafast glutamate sensor.[21] Furthermore, as described in more detail later, the sensor is implanted at the layer 4 of the visual cortex next to the direct thalamocortical projection, where a small concentration of glutamate is released by different types of visual stimulation. In this case, the response time and low detection limit of our sensor are suitable to detect the glutamate release. However, even faster response times, sensitivity, and better resolution for transient glutamate detection can be achieved by optimizing the Nafion layer dimensions in future studies, as shown theoretically by Clay et al.[60]

Phase Evolution in Nickelate Sensors after Exposure to Glutamate Dosages. The hydrogen peroxide oxidation reaction at the nickelate electrode can be monitored via the electrochemical station. Separately, the nickelate thin film can be studied post-reaction by ex situ methods using high-energy resolution synchrotron radiation. The resistance evolution of the films (I−V curves) after the treatment with different dosages of glutamate in 0.01 M PBS (pH 7.4) solution (Figure 2d) is shown in Figure 2e. The pristine metallic NNO film has a low resistivity of ~0.18 mΩ cm. The 1× dosage of glutamate leads to a slight increase to around 0.25 mΩ cm. The 2× and 3× dosage treatment further results in substantial change in the resistivity by ~5× and ~2 orders of magnitude. Such PBS-mediated conductivity reduction due to electron filling is nonvolatile at ambient conditions.

To investigate the mechanism of sensor response to glutamate, microstructural and electronic structure studies were performed on representative samples. Synchrotron X-ray diffraction curves taken from films after different dosage treatments are shown in Figure 2f. The pristine NNO was epitaxially grown on the single crystalline LAO substrate, which shows a shoulder (220) diffraction peak (orthorhombic notation) at $Q_z \approx 3.27$ Å^{-1}. The substrate LAO(002) diffraction peak (in pseudocubic notation) is located at 3.31 Å^{-1}, indicating the NNO films' larger out-of-plane lattice parameter. Upon 1× dosage glutamate treatment, the diffraction peak of NNO becomes broader and shows a shift toward lower Q_z position, which arises from the proton/electron doping-induced lattice expansion and distortion. The XRD pattern of NNO after further 2× dosage and 3× dosage treatments demonstrates no apparent diffraction peak, which indicates a decrease in the film crystallinity due to the greater concentration of protons that are intercalated through the film. Synchrotron X-ray absorption near-edge spectroscopy (XANES) measurements near the O K-edge of NNO films after different dosages are shown in Figure 2g. The gradual
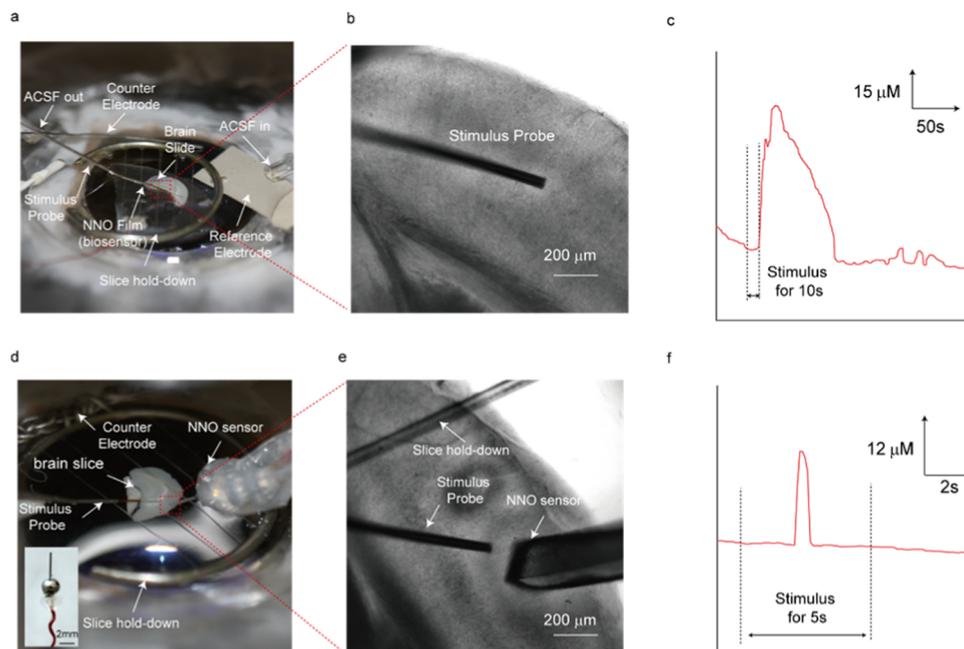
Figure 3. *Ex vivo* studies of glutamate release in stimulated brain slices. (a) *Ex vivo* stimulated glutamate sensing setup using a visual cortex brain slice of a mouse. The size of the visual cortex brain slice is ~0.46 cm × 0.76 cm. (b) Zoom-in image of the brain slice with the electrical stimulus probe is attached. (c) Representative *ex vivo* stimulated glutamate sensing curve is shown. The glutamate sensing experiment was performed using a three-electrode setup at 0.6 V *vs* Ag/AgCl. A sharp current peak was observed ~8 s after the electrical stimulus (500 μA 0.1 ms width pulse, 40 Hz for 10 s) was applied to the brain slice. (d) Same setup shown in (d) is identical to (a). Here, the glutamate sensor was machined into a needle-shape probe and was inserted into the brain slice. (e) Zoom-in image of the brain slice with the stimulus probe and the glutamate sensor. (f) Representative *ex vivo* stimulated glutamate sensing curve recorded by the needle-shape sensor. The recording and stimulation protocol is the same as in (a)−(c), but the stimulation time is 5 s. The peak was detected ~2 s after the electrical stimulus was turned on.

suppression of the O K-edge absorption peak at 529 eV occurs upon different dosage treatment, suggesting a decrease in oxygen-projected density of unoccupied states owing to the electron injection into O_{2p}−Ni_{3d} hybridized orbitals. Synchrotron XANES measurements near the Ni K-edge of NNO films after different dosages measured at different incidence angles are shown in Figure 2h,i. The choice of incidence angles allows us to determine if there are any significant changes occurring only near the surface as opposed to a significant fraction of the film thickness. The pre-edge region (shown in the inset of Figure 2h,i) of XANES can be regarded as the fingerprint of the covalence status between the O_{2p}−Ni_{3d} hybridized orbital. The intensity of the white line peak depends on the occupancy of the bound final states. Both spectra at incidence angles of 0.3 and 5.2° show similar evolution trend that the white line peak amplitude significantly gets weaker and the effective integrated area underneath the pre-edge peak apparently gets suppressed after the glutamate treatment. Both reductions indicate electron filling into the hybridized d-orbital due to the neurotransmitter. The reduction in the integrated pre-edge peak area of glutamate-treated NNO is normalized by the area of pristine NNO. For an incidence angle of 0.3°, the pre-edge area decreases by 48% for the 3× dosage treatment (Table S2). In comparison, such change is estimated to be 28% for an incidence angle of 5.2° (Table S3). The previous work using $SmNiO_3$ thin films for spontaneous transfer of hydrogen from glucose (with no electrical stimuli) showed only near-surface doping to a few unit cells.[10] In this work, we can see that electron filling from a neurotransmitter could be a bulk effect across the film thickness under the electrochemical bias used in the amperometric sensing methodology, confirmed by both synchrotron XRD and XANES measurements as shown above.

To verify reproducibility, we annealed the sensor devices to remove the doped hydrogen, started the fabrication process from scratch for subsequent reuse (Figure S8).

Ex Vivo Studies of Neurotransmitter Release from the Mouse Visual Cortex. Prior to demonstrating the use of these biosensors for real-time monitoring of neurotransmitter glutamate released from the neuronal tissue of living animals, we first measured glutamate release in acute mouse brain slices *ex vivo*. Brain slices were prepared from the primary visual cortex (V1) of mice. In each experiment, a glutamate NNO sensor was placed underneath a brain slice and secured by a slice holder for glutamate measurement. To stimulate glutamate release from the presynaptic terminals within the slice, a bipolar stimulus electrode was placed on the surface of the layer 4 of the cortical slice. Electrical pulses were applied as described in Methods (Figure 3a,b). Stimulation of layer 4, the main recipient of the thalamic input, was justified by the anatomical organization of the V1 microcircuit and the extensive previous studies of the long-term synaptic plasticity at the layer 4 to layer 2/3 synapse.[61] Furthermore, this layer 4 to layer 2/3 synapse represents one of the strongest feedforward inputs in the cortical column. To achieve full contact of the brain tissue with the biosensor, we made sure that the sensor was about twice as large as the brain slice (0.46 × 0.76 cm^2) (Figure 3a). When the glutamate reached the glutamate oxidase layer of the biosensor, the redox current was captured by the perovskite nickelate biosensor. The sampling rate for the redox current recording was 10 Hz, and all of the current density shown in Figure 3c,f is normalized to square millimeter to compare the data obtained with sensors of different surface areas. About 8 s following the onset of electrical stimulation (500 μA 0.1 ms width pulse, 40 Hz for 10
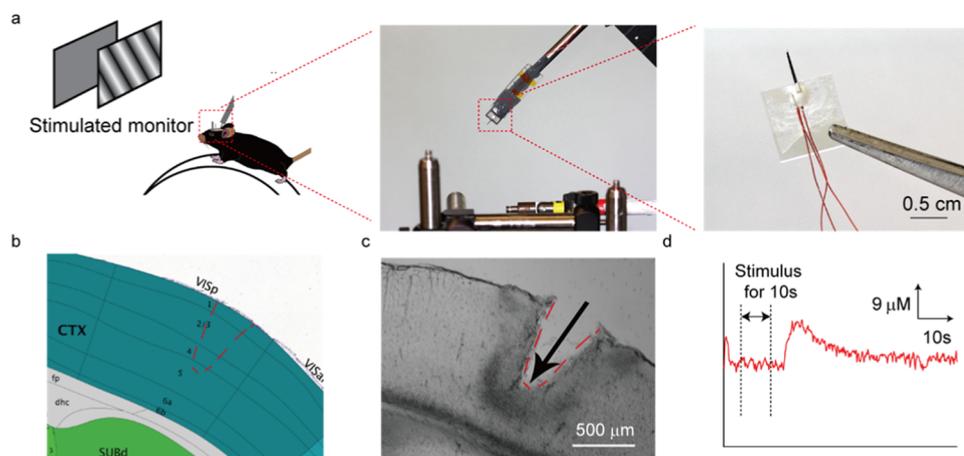
Figure 4. *In vivo* glutamate release studies on awake mice. (a) Setup for the *in vivo* glutamate sensing from awake, head-fixed mouse and close-up images of the sensor used. The visual stimulus presented was drifting sinusoidal grating (spatial frequency = 0.03 cpd, temporal frequency = 3 Hz, and speed = 100°/s) presented for 10 s with an intertrial delay of 8 s where a gray screen was displayed. (b) Mouse brain atlas (from Allen Brain Institute) showing the sensor was inserted into the binocular V1 region of the primary visual cortex (V1) outlined in the red dashed line. (c) Slice histology showing the insertion path of the sensor in V1. (d) Representative *in vivo* glutamate recording is shown during visual stimulus made by the glutamate sensor (red).

s), the peak current density per mm^2 is up to 20 nA (baseline-subtracted), indicating that the highest glutamate concentration recorded is about 60 μM (Figure 3f). The baseline is the average current density value when no prominent current peak is detected in consecutive 20 s of a recording trial. The results suggest that NNO can be successfully used for sensing the glutamate signal *ex vivo*.

The large surface area of the sensor increased the sensitivity of glutamate detection, but its size limited the spatial resolution. Furthermore, the size of the sensor was prohibitively large for *in vivo* recordings from the live mouse. To develop a more compact sensory design that could be inserted into the brain of a live mouse, we developed a needle-like prototype of the biosensor with the 250 × 300 μm^2 dimensions. Although it is larger than the latest state-of-the-art silicon probe for electrophysiological recordings, this design represented a major improvement compared to the benchtop version and could be successfully used for the recordings. Before using the new design *in vivo*, we first tested it in brain slices. We had placed the new needle-shape sensor on the top of layer 2/3 and successfully recorded glutamate release when applying the same high-frequency stimulation (500 μA 0.1 s width pulse, 40 Hz for 5 s) of layer 4 in V1 as described earlier (Figure 3d−f). The current density peak was detected about 2 s after the stimulation began, the peak is up to 7 nA/mm^2, which corresponds to >21 μM of glutamate during this experiment (Figure 3f). The faster and more transient response detected by the needle-shape sensor compared to the large baseplate sensor could be explained by the closer proximity of the needle-shape sensor to the presynaptic terminals in layer 2/3 releasing glutamate directly compared to the slow excessive glutamate spillover required to reach the baseplate sensor. The results indicate that the needle-like sensor is more precise and sensitive and is promising for glutamate monitoring in living animals.

In Vivo Studies of Neurotransmitter Release from the Mouse Brain. To demonstrate the potential for real-time biological applications, the nickelate−Nafion sensors were used to record glutamate release *in vivo* in awake, head-fixed mice. A needle-shaped version of the sensor was inserted into the binocular region of the visual cortex to record the release of glutamate in response to visual stimulation (Figure 4). The experiment setup and mouse brain atlas (from Allen Brain Institute[62]) are shown in Figure 4a,b, respectively. Figure 4d shows the measured response to the drifting sinusoidal grating (spatial frequency (SF) = 0.03 cycles/deg (cpd), temporal frequency (TF) = 3 Hz, and speed = 100°/s) presented for 10 s. The sensor with the coating shows a stimulus-induced peak, suggesting that it is detecting extracellular glutamate. Recordings made in response to other visual stimuli patterns are shown in Figure S9. Some differences in the amount of glutamate detected may be potentially explained by the differences in the ability of different visual stimulation protocols to activate presynaptic terminals in the visual cortex and release glutamate. To compare *in vivo* glutamate release in response to visual stimulation to the standard electrophysiological recordings performed in mice, we performed extracellular recordings of visually evoked potentials (VEPs) and neuronal unit responses as described previously (Figure S10).[63]

There was a temporal delay between stimulation and glutamate detection both *ex vivo* and *in vivo*. This delay was higher than the response latency in extracellular electrophysiological recordings of local field potentials (LFPs) and neuronal spikes (Figure S10). The distinct behavior may be potentially explained by the action of the glutamate transporters in the presynaptic terminal and astrocytes, which can swiftly remove glutamate from the synaptic cleft and extracellular space following visual stimulation. Consequently, we may be able to detect only excess glutamate released following extensive, prolonged electrical stimulation in brain slices or visual stimulation *in vivo*. The slow diffusion of this excess glutamate may also explain the latency between the stimulation and the glutamate signal detection by the biosensor compared to electrophysiological methods. Future studies can include further miniaturization of electrode devices for multiplexed long-term *in vivo* brain research and biocompatibility analysis.

■ CONCLUSIONS

We have presented the demonstration of an amperometric biosensor using a correlated metallic perovskite nickelate (*i.e.*, $NdNiO_3$ (NNO)) for neurotransmitter sensing in both *ex vivo* brain slices and *in vivo* inside the brain of awake mice. The biosensor consists of a NNO/Nafion/GluO$_x$ heterostructure with a high selectivity toward glutamate, fast response time (1.2 s), and low detection limit (16 nM). Correlated metallic systems interfaced with polymers can therefore contribute to design of components for neurotransmitter sensing and brain—machine interfaces.

■ METHODS

Fabrication of NdNiO$_3$ (NNO)/Nafion/Enzyme Heterostructures. *NdNiO$_3$ Film Deposition.* Perovskite nickelate NdNiO$_3$ (NNO) thin films were grown on single-crystal (001) LaAlO$_3$ (LAO) substrates (MTI Corp.) using a AJA UHV magnetron sputtering at room temperature. All substrates were rinsed by toluene, acetone, and isopropyl alcohol and dried with high-purity N$_2$ before deposition. The optimized growth condition was calibrated using a Phenom scanning electron microscope (SEM) equipped with energy-dispersive X-ray spectroscopy (EDS). The deposition gas atmosphere is a mixture of 40/10 sccm Ar/O$_2$ at a total deposition background pressure of 5 mTorr. Two metallic Ni (DC, 66 W) and Nd (radio frequency (RF), 145 W) targets were used for deposition. The film growth rate is ~2.5 nm/min. After deposition, the samples were treated by post-annealing in air at 500 °C for 24 h in a tube furnace with a ramping and cooling rate of 1.5 °C/min. Films with a thickness of ~50 nm were used in this work.

Nafion Coating Synthesis. Perovskite nickelate NdNiO$_3$ (NNO) thin films were used as a working electrode for neurotransmitter detection (image shown in Figure S1). The films were connected using a magnetic wire (34 AWG, Digi-Key Corp., MN) by silver paste. The contact was insulated using poly(dimethylsiloxane) (PDMS) leaving only the working area open for electrochemical activity. The thin-film electrode was then coated with a thin layer of Nafion as a permselective membrane to improve the selectivity for glutamate over other interferences such as ascorbic acid (AA), acetaminophen (AC), and uric acid (UA). Prior to coating, thin-film electrodes were baked at 175 °C for 4 min to remove any moisture. They were then removed from the oven and lowered into the amber vial containing Nafion solution, such that the recording sites were submerged in the solution. The films were rotated in a circular motion five times (~1 s per rotation). The films were removed from the Nafion solution and baked at 175 °C for 4 min. They were removed from the oven and cooled down for at least 10 min at room temperature before coating with the GluO$_x$ enzyme for glutamate sensing.

Enzyme Immobilization. After Nafion coating, the films were functioned with glutamate oxidase (GluO$_x$), bovine serum albumin (BSA), and glutaraldehyde protein matrix. BSA (2.5%) and glutaraldehyde (0.4%) were added to the microcentrifuge tube containing glutamate oxidase (500 U/mL). The solution was mixed by centrifuging for 30 s. The resulting solution was 1% BSA, 0.15% glutaraldehyde, and 100 U/mL GluO$_x$. GluO$_x$ was cross-linked with BSA and glutaraldehyde to be immobilized on the surface of the Nafion-coated film. The protein matrix solution was used immediately. A 0.1−10 μL micropipette was used to coat the NNO sensor. Two micrometers of the glutamate matrix was drawn up. A small droplet of the solution was formed at the pipet tip without completely releasing the droplet. The solution droplet was then lowered to briefly contact the film surface and is raised straight up and off the NNO sensor surface. This was repeated four times with at least 1 min wait in between. The coating films were cured at room temperature from 48 to 72 h and then stored at 4 °C before first measurement.[19,64]

Chemical Agent Procurement. Glutamate oxidase (GluO$_x$) from *Streptomyces* with a rated activity of 25 units/mg protein was obtained from Cosmo Bio USA (Carlsbad, CA). Nafion perfluorinated resin solution (5 wt % in water and alcohol) and glutaraldehyde (25% in water) were obtained from Sigma-Aldrich (St. Louis, MO). L-Glutamic acid and 0.1 M phosphate-buffered saline (PBS, pH 7.4) were obtained from Fisher Scientific (Waltham, MA). Ascorbic acid (AA), uric acid (UA), and acetaminophen (AC) were purchased from Alfa Aesar (Fisher Scientific, Waltham, MA). Elastomeric poly-(dimethylsiloxane) (PDMS, Sylgard 184) was purchased from Dow Corning (Midland, MI). Water was purified by Milli-Q (Millipore, Bedford, MA). The Ag/AgCl/NaCl (3.5 M) reference electrode (RE) was acquired from Bio-Logic USA (LLC, Knoxville, TN) for three-electrode measurements.

Microscopy. Cross-sectional area images of the NNO/LAO film were obtained using a Cs and Cc aberration double-corrected FEI Titan transmission electron microscope (TEM) at 200 keV. The TEM specimen was prepared by focused ion beam (FIB) lift-out and subsequently milled in a Gatan PIPS at 200 eV to remove any excess damage layers introduced by the FIB. The scanning TEM energy-dispersive X-ray spectroscopy (STEM-EDS) data was collected using an FEI Talos equipped with a Super X EDS at 200 keV.

Electrical Conduction Measurements. After each glutamate treatment, the NNO film (without Nafion coating) was rinsed with DI water and dried with high-purity N$_2$ gas. Two Pd pads with a thickness of 100 nm were deposited onto the film as contact using magnetron sputtering from the Pd target. The current−voltage (I−V) curves were measured between two Pd contacts using a Keithley 2635A source measure unit. For measurements of the in-plane conductivity of the film, the cyclic voltammetry measurement was performed using a three-electrode setup on a Solatron 1260 potentiostat. A silver paste was scratched into a corner of the NNO film (5 mm × 10 mm), and a stainless-steel wire was in contact with Ag paste and baked at 50 °C until the paste become solid. Thereafter, the back, sides, and Ag paste area were sealed with inert epoxy (Locite 9460) leaving the NNO film (~0.3 cm^2) exposed to the electrolyte only. In our measurement, the NNO film served as the working electrode and the Pt wire and Ag/AgCl in 3.5 M KCl served as the counter electrode (CE) and the reference electrode, respectively. To the 0.1 M KCl electrolyte, 5×10^{-3} M each of K$_3$Fe(CN)$_6$ and K$_4$Fe(CN)$_6$·3H$_2$O (Sigma, >99%) was added. Before measurement, the electrolyte was bubbled with ultra-high-purity N$_2$ for 30 min.

Synchrotron X-ray Measurements. The X-ray measurements were carried out on beamline 33-ID-D at Advanced Photon Source, Argonne National Laboratory. A six-circle Newport Kappa diffractometer was used for the X-ray diffraction measurement near the substrate (002) Bragg peak. The nominal incident X-ray photon energy of 8.333 keV was used for the XRD measurements, which is lower than the measured Ni absorption edge of ~8.345 keV. XRD and XANES measurements were done on the same spot of the sample. For the XAS measurement, a single element Vortex detector was used to collect the fluorescence signal from the sample as the incident X-ray energy was scanned through the Ni K absorption edge (8.31−8.56 keV). Two different incident angles of X-rays were chosen for the XAS measurements: one at 5.2° to survey the whole depth of the film and another at 0.3°, *i.e.*, below the critical angle, where the X-ray extinction depth is reduced to less than 10 nm, to probe the Ni cation valence state of the surface layer. O K-edge X-ray absorption spectroscopy was conducted at beamline 29-ID IEX at the Advanced Photon Source, Argonne National Laboratory. Data were collected in a pressure better than 1×10^{-8} Torr in total fluorescence yield (TFY) using a microchannel plate with 7° angular acceptance located at $2\theta = 20°$. We used circular polarization with an overall energy resolution better than 100 meV. The incidence angle was set to $\theta = 5°$, as to limit the penetration depth to 10 nm at the O K-edge. The total fluorescence yield was normalized by the incident X-ray intensity (I_0) using the drain current from a gold mesh upstream of the sample.

Atomic Force Microscopy (AFM). The topographic AFM mapping of the NNO films upon different glutamate treatments was performed using an Asylum MFP3D stand-alone atomic force microscope using Asylum ASYELEC-01 conductive tips (Si coated with Ti/Ir).

Ex Vivo Glutamate Sensing Experiments on Brain Slices. *Needle-Shape NNO/LAO Electrode Fabrication.* The needle-shape NNO/LAO electrodes used in the *ex vivo* experiments were fabricated

by using a wafer saw to cut the NNO/LAO wafer into $1 \times 10 \text{ mm}^2$ needle-like structures. The electrodes were then mechanically polished with the 3 μm polishing paper such that the width was approximately the same as the original wafer thickness (250 μm) resulting in a $0.25 \times 0.25 \times 10 \text{ mm}^3$ final structure.

Animals and Acute Brain Slices Preparation. All animal procedures were approved by the Purdue University Animal Care and Use Committee. Brain slices were prepared as described.[65] P28–P35 female C57BL/6 mice were anesthetized with the mix of 90 mg/kg of ketamine and 10 mg/kg of xylazine delivered by intraperitoneal injection. After confirmation of deep anesthesia, transcardiac perfusion was performed with oxygenated (carbogen from Airgas: 95% O_2, 5% CO_2) high sucrose dissection buffer (HSDB, composition in millimolar: 1.25 NaH_2PO_4, 25 $NaHCO_3$, 212.7 sucrose, 10 dextrose, 2.5 KCl, 0.5 $CaCl_2$, 7 $MgCl_2$, and 1.3 ascorbic acid). After the perfusion has completed, the brain was quickly isolated by dissection. The brain was trimmed to the desirable shape and fixed in the cutting chamber of the vibratome (Leica VT1000) filled with the HSDB while constantly oxygenated with carbogen flow. The coronal brain slices containing the striatum and primary visual cortex (V1) were cut into 300 μm thick sections. The brain slices were transferred immediately to a 32 °C incubation chamber containing oxygenated artificial cerebrospinal fluid (ACSF, composition in mM: 124 NaCl, 2.5 KCl, 2 $CaCl_2$, 0.8 $MgCl_2$, 1.23 NaH_2PO_4, 26 $NaHCO_3$, and 10 glucose) and incubated there for 30 min. The slices were then kept at room temperature (about 25 °C) for at least 1 h before use.

Electrical Stimulation of Brain Slices. The electric current was generated by a stimulation isolator (WPI A365) and output to a bipolar electrode (FHC CE2C55). The thin tip of the bipolar electrode was placed on the surface of the target brain areas. To induce glutamate release in V1, 5 or 10 s constant 40 Hz stimulations were applied; the width of one pulse was 0.1 ms, the amplitude was 500 μA.

Ex Vivo Experiment Setup. For *ex vivo* experiments shown in Figure 3a, a piece of NNO/LAO was fixed on the experiment platform, on which the brain slide was placed. Pt wire and Ag/AgCl were served as the counter electrode and the reference electrode, respectively. During the experiment, the recording chamber was continuously perfused with an oxygenated ACSF solution. A slide hold-down was placed to avoid slice movement during measurements. The *ex vivo* experiment shown in Figure 3d shared the same setup. Alternatively, a needle-shape NNO/LAO connected *via* a magnetic wire (30 AWG, Digi-Key Corp., MN) by a solder served as the working electrode. PDMS was used as an insulation layer over the solder connection to prevent any contact with the solution. The device was then attached to a stainless tube for insertion.

Ex Vivo Electrochemical Evaluation. Electrochemical sensing experiments were carried out using a SP-200 potentiostat (Bio-Logic USA, LLC, Knoxville, TN). Investigation of glutamate detection was done through the chronoamperometry $I-t$ curve technique. All chronoamperometry data were collected after 20 min of settling time unless stated otherwise. A conventional three-electrode cell was used for chronoamperometry measurements with Ag/AgCl/NaCl (3.5 M) as the reference electrode and the graphite rod as the counter electrode for all evaluations. Parameters for chronoamperometry were at 0.6 V *vs* Ag/AgCl with 0.1 s sampling interval. All chronoamperometry was performed in a stirring solution of 0.01 PBS (pH 7.4) as the supporting electrolyte and a rotation rate of 180 rpm.

In Vivo Glutamate Sensing Experiments on Awake Mice.
Fabrication of In Vivo Sensors. A complete three-electrode chemical sensor system was prepared for *in vivo* brain implantation experiments (image shown in Figure S2). The shank was prepared by spin coating SU-8 2050 resin (MicroChem, Newton, MA) on a 4 in. silicon wafer substrate with 3500 rpm of spin speed to obtain 50 μm of thickness. The sample was soft-baked for 3 min at 65 °C and 6 min at 95 °C. UV light (dose: 160 mJ/cm^2) was exposed using a mask aligner (Suss MA6, Suss MicroTech, Garching, Germany). Post-exposure bake was done for 1 min at 65 °C and 6 min at 95 °C. The sample was

developed in the SU-8 developer (MicroChem, Newton, MA) for 5 min and rinsed with isopropyl alcohol. Hard bake was done at 200 °C for 10 min. Shanks were released from the silicon wafer by etching the natural oxide with buffered oxide etch followed by rinsing in DI water for five times.

After fabricating the desired SU-8 shank structure, the platinum nanoparticle nanocomposite was printed on the backside of the shank as the CE and as a conductive trace for the RE on the front side.[64] Ag/AgCl ink was used to print the RE on top of the conductive trace in the front of the shank. Silver ink was printed as contact pads, and PDMS was printed as an insulated layer exposing only the electrodes and contact pads. A three-axis microfluid dispensing robot (Pro-EV 3, Nordson EFD, East Providence, RI) was used for the printing process. The needle-shape NNO/LAO was then attached right below the reference electrode and connected *via* a magnetic wire (34 AWG, Digi-Key Corp., MN) by silver ink. The whole system was placed on a bared LAO substrate (1 cm $\times$ 1 cm) before attached to a stainless-steel tubing, which helps guide the insertion (Figure 4a).

Mice and Surgical Procedures. Surgical procedures were performed as described previously.[66] C57BL/6 mice were housed on a 12 h light/dark cycle. P55 old mice were anesthetized with 5% inhaled isoflurane (in oxygen) and maintained at 1.5% during surgery. Once deep anesthesia was confirmed, the mice were affixed with ear bars to a Neurostar stereotaxic surgery frame and ophthalmic ointment was applied to the eyes. The scalp was shaved and sterilized with Dynarex ethanol wipes before a midline incision was made and expanded to uncover the lambda and bregma skull sutures. The skull was sterilized using 3% H_2O_2, and the periosteum was removed. Once the skull was dry, coordinates for the binocular visual cortex (from lambda: AP 0.8 mm, ML $\pm$3.2 mm) were marked using Neurostar stereodrive software. A 9.5 mm long head post was glued in place with cyanoacrylate to a point on the midline of the skull 3.5 mm anterior to bregma. A reference pin made from a 1.5 mm tungsten wire soldered to the end of a 0.79 mm diameter gold-plated pin was also glued into place with cyanoacrylate after insertion through the skull at a point on the midline 0.2 mm anterior of bregma. Metabond bone cement was used to seal the skull under a head cap.

Habituation of the mice to the head-fixation apparatus began after a day of recovery from the initial surgery. Habituation lasted for a minimum of 3 days for 90 min/day. When attached to the head-fixation apparatus via the implanted head post, the mice stood on a vertical treadmill facing the center of a 47.63 cm $\times$ 26.99 cm monitor screen placed 16.51 cm in front of them. After the last day of habituation, the following day, a craniotomy was performed at one of the marked coordinates. The same method of anesthesia was used for this surgery, as for the initial head post-implantation. Once affixed to the head-fixation apparatus, the biosensor was inserted normal to the surface of the now exposed binocular area of the primary visual cortex. Once inserted, the sensor was allowed to settle and the mouse allowed to fully awaken from anesthesia over 30 min before recording. For the electrophysiology data, the process was the same as with the biosensor, but instead, a 64 channel silicon electrode was inserted. After a recording session, the craniotomy was resealed with the Kwik-Cast silicone elastomer and Ortho-Jet orthodontic acrylic resin.

Visual Stimulation. To generate and present the visual stimuli, the open-source psychology software PsychoPy was used. During the habituation of the mice, they were shown a control screen made with the color space "gray" on a monitor with a mean luminance of 73 cd/m^2. The visual stimuli provided to promote a neural response were single 10 s sinusoidal drifting gratings (spatial frequency (SF) = 0.03 cpd of visual angle, temporal frequency (TF) = 3 Hz, and speed = 100°/s, oriented and drifting at an angle of 150°) with an intertrial interval of 8 s, a drifting checkerboard pattern (temporal frequency (TF) = 3 Hz and speed = 100°/s, oriented and drifting at an angle of 150°) displayed for 10 s with an intertrial interval of 8 s as well as a 10 s display time with an intertrial interval of 30 s, and a full contrast modulation following a 2.5 Hz square wave displayed for 10 s with an intertrial interval of 60s.

Perfusions and Histology. Before starting the perfusion, the mice were anesthetized with intraperitoneal injections of a 90 mg/kg of

ketamine and 10 mg/kg of xylazine solution. The inner cavity of the peritoneum was exposed with an incision under the rib cage before cutting the lateral sides of the rib cage and removing the diaphragm. The heart was then exposed by peeling back the rib cage and any other connective tissue. 1× PBS was gravity-fed through a 25-gauge needle inserted into the left ventricle to force blood out of an incision made in the right atrium. Perfusion of 4% paraformaldehyde (PFA) was then used to fix the tissue. To remove the brain, the animal was decapitated and the head cap sealing the skull was removed. Then, cuts were made up the midline and along the lambda and bregma sutures to remove the skull and expose the brain enough to remove it from the skull. Once extracted, the brain was placed in 4% PFA for 24 h before slicing it into 100 μm thick coronal sections. The slices were carefully attached on slides and mounted by *N*-propyl gallate (NPG)−glycerol. The sensor track was then visualized by light microscopy.

Analysis of Electrophysiological Data. Raw traces were digitized at 30 kHz and acquired with OpenEphys acquisition hardware and software. For LFP analysis, the raw signal traces were filtered (1−300 Hz) and downsampled to 1 kHz, manually inspected for artifacts, and filtered with a notch filter removing 60 Hz noise. To compare LFPs between mice, the first and strongest trial-averaged visually evoked potential (VEP) from a visual stimulus (putative layer 4 VEPs) from each column of a silicon probe was used. For spike analysis, raw traces were bandpass-filtered (300−6000 Hz). Spikes were detected and sorted with the use of Kilosort, a template-based clustering algorithm implemented in Matlab.[67] The default Kilosort parameters were used except for a six spike detection (SD) threshold for spike detection and initializing the templates from data. Manual inspection of the resulting clusters for unit quality was performed using the Phy template GUI, based on the criteria[68] that have been previously described.[66]

Single-Unit Analysis. To analyze single-unit activity, they were put into peristimulus time histograms (PSTHs) with a 10 ms bin size and were smoothed with a Gaussian smoothing kernel (width = 100 ms). *z*-Score heatmaps were made by normalizing to the mean firing rate (FR) across time, so $z = (FR - \text{mean FR})/(\text{SD FR})$, and the *z*-scores of the population time course line plots were made by normalizing FR to the baseline period preceding stimuli presentation, so $z = (FR - \text{mean baseline FR})/(\text{SD baseline FR})$.

■ ASSOCIATED CONTENT

ⓢ Supporting Information

The Supporting Information is available free of charge at https://pubs.acs.org/doi/10.1021/acsami.0c02826.

Photograph of the NNO-based glutamate biosensor; photograph of the needle-shape NNO-based glutamate biosensor; AFM image of the Nafion/NNO film; cyclic voltammetry (CV) scan of the NNO-based glutamate biosensor in different solutions; control *C−V* measurement with the NdNiO₃ electrode; amperometric sensing and interference (selectivity) studies of the nickelate−Nafion heterostructure; sensor performance measurements; recovery and reuse of the treated NNO biosensor; *in vivo* glutamate sensing in awake mice exposed to various visual stimuli; electrophysiology experiments in awake mice with silicon probes (control); summary of the film thickness; summary of the normalized pre-edge area of Ni K-edge XANES at incidence angles of 0.3 and 5.2° (PDF)

■ AUTHOR INFORMATION

Corresponding Authors

Yifei Sun − *School of Materials Engineering, Purdue University, West Lafayette, Indiana 47907, United States;* ⓘ orcid.org/0000-0002-2346-8402; Email: yifeisun1@hotmail.com

Shriram Ramanathan − *School of Materials Engineering, Purdue University, West Lafayette, Indiana 47907, United States;* Email: shriram@purdue.edu

Hyowon Lee − *Birck Nanotechnology Center, Center for Implantable Device, Weldon School of Biomedical Engineering, Purdue University, West Lafayette, Indiana 47907, United States;* ⓘ orcid.org/0000-0001-7628-1441; Email: hwlee@purdue.edu

Alexander A. Chubykin − *Department of Biological Sciences, Purdue Institute for Integrative Neuroscience, Purdue University, West Lafayette, Indiana 47907, United States;* Email: chubykin@purdue.edu

Authors

Tran N. H. Nguyen − *Birck Nanotechnology Center, Center for Implantable Device, Weldon School of Biomedical Engineering, Purdue University, West Lafayette, Indiana 47907, United States*

Adam Anderson − *Department of Biological Sciences, Purdue Institute for Integrative Neuroscience, Purdue University, West Lafayette, Indiana 47907, United States*

Xi Cheng − *Department of Biological Sciences, Purdue Institute for Integrative Neuroscience, Purdue University, West Lafayette, Indiana 47907, United States*

Thomas E. Gage − *Center for Nanoscale Materials, Argonne National Laboratory, Lemont, Illinois 60439, United States*

Jongcheon Lim − *Birck Nanotechnology Center, Center for Implantable Device, Weldon School of Biomedical Engineering, Purdue University, West Lafayette, Indiana 47907, United States*

Zhan Zhang − *X-ray Science Division, Advanced Photon Source, Argonne National Laboratory, Lemont, Illinois 60439, United States*

Hua Zhou − *X-ray Science Division, Advanced Photon Source, Argonne National Laboratory, Lemont, Illinois 60439, United States*

Fanny Rodolakis − *X-ray Science Division, Advanced Photon Source, Argonne National Laboratory, Lemont, Illinois 60439, United States*

Zhen Zhang − *School of Materials Engineering, Purdue University, West Lafayette, Indiana 47907, United States*

Ilke Arslan − *Center for Nanoscale Materials, Argonne National Laboratory, Lemont, Illinois 60439, United States*

Complete contact information is available at:
https://pubs.acs.org/10.1021/acsami.0c02826

Author Contributions

Y.S., T.N.H.N., and A.A. contributed equally to this work. Y.S., T.N.H.N., A.A., X.C., and Z.Z. contributed to fabricating the samples and conducted the measurement and data analysis of all experiments. T.E.G. and I.A. conducted the TEM characterization and needle electrode preparation. Z.Z., H.Z., and F.R. conducted the X-ray diffraction and X-ray absorption measurments. S.R., H.L., and A.A.C. conceived and designed the project. All authors contributed to writing the paper.

Notes

The authors declare no competing financial interest.

■ ACKNOWLEDGMENTS

■ REFERENCES

(1) Catalano, S.; Gibert, M.; Fowlie, J.; Iniguez, J.; Triscone, J.-M.; Kreisel, J. Rare-Earth Nickelates $RNiO_3$: Thin Films and Hetero-structures. *Rep. Prog. Phys.* **2018**, *81*, No. 046501.

(2) Wang, L.; Stoerzinger, K. A.; Chang, L.; Zhao, J.; Li, Y.; Tang, C. S.; Yin, X.; Bowden, M. E.; Yang, Z.; Guo, H.; et al. Tuning Bifunctional Oxygen Electrocatalysts by Changing the a-Site Rare-Earth Element in Perovskite Nickelates. *Adv. Funct. Mater.* **2018**, *28*, No. 1803712.

(3) Scherwitzl, R.; Zubko, P.; Lezama, I. G.; Ono, S.; Morpurgo, A. F.; Catalan, G.; Triscone, J. M. Electric-Field Control of the Metal-Insulator Transition in Ultrathin $NdNiO_3$ Films. *Adv. Mater.* **2010**, *22*, 5517−5520.

(4) Catalan, G. Progress in Perovskite Nickelate Research. *Phase Transitions* **2008**, *81*, 729−749.

(5) Middey, S.; Chakhalian, J.; Mahadevan, P.; Freeland, J.; Millis, A. J.; Sarma, D. Physics of Ultrathin Films and Heterostructures of Rare-Earth Nickelates. *Annu. Rev. Mater. Res.* **2016**, *46*, 305−334.

(6) Catalan, G.; Bowman, R.; Gregg, J. Transport Properties of $NdNiO_3$ Thin Films Made by Pulsed-Laser Deposition. *J. Appl. Phys.* **2000**, *87*, 606−608.

(7) Alsaqqa, A. M.; Singh, S.; Middey, S.; Kareev, M.; Chakhalian, J.; Sambandamurthy, G. Phase Coexistence and Dynamical Behavior in $NdNiO_3$ Ultrathin Films. *Phys. Rev. B: Condens. Matter Mater. Phys.* **2017**, *95*, No. 125132.

(8) Hauser, A. J.; Mikheev, E.; Moreno, N. E.; Hwang, J.; Zhang, J. Y.; Stemmer, S. Correlation between Stoichiometry, Strain, and Metal-Insulator Transitions of $NdNiO_3$ Films. *Appl. Phys. Lett.* **2015**, *106*, No. 092104.

(9) Wang, L.; Stoerzinger, K. A.; Chang, L.; Yin, X.; Li, Y.; Tang, C. S.; Jia, E.; Bowden, M. E.; Yang, Z.; Abdelsamie, A.; et al. Strain Effect on Oxygen Evolution Reaction Activity of Epitaxial $NdNiO_3$ Thin Films. *ACS Appl. Mater. Interfaces* **2019**, *11*, 12941−12947.

(10) Zhang, H.-T.; Zuo, F.; Li, F.; Chan, H.; Wu, Q.; Zhang, Z.; Narayanan, B.; Ramadoss, K.; Chakraborty, I.; Saha, G.; et al. Perovskite Nickelates as Bio-Electronic Interfaces. *Nat. Commun.* **2019**, *10*, No. 1651.

(11) Okumoto, S.; Looger, L. L.; Micheva, K. D.; Reimer, R. J.; Smith, S. J.; Frommer, W. B. Detection of Glutamate Release from Neurons by Genetically Encoded Surface-Displayed Fret Nano-sensors. *Proc. Natl. Acad. Sci. U.S.A.* **2005**, *102*, 8740−8745.

(12) Behar, K. L.; Rothman, D. L. In Vivo Nuclear Magnetic Resonance Studies of Glutamate-Γ-Aminobutyric Acid-Glutamine Cycling in Rodent and Human Cortex: The Central Role of Glutamine. *J. Nutr.* **2001**, *131*, 2498S−2504S.

(13) Liu, D.; Thangnipon, W.; McAdoo, D. J. Excitatory Amino Acids Rise to Toxic Levels Upon Impact Injury to the Rat Spinal Cord. *Brain Res.* **1991**, *547*, 344−348.

(14) Weltin, A.; Kieninger, J.; Urban, G. A. Microfabricated, Amperometric, Enzyme-Based Biosensors for in Vivo Applications. *Anal. Bioanal. Chem.* **2016**, *408*, 4503−4521.

(15) Shen, J. Impaired Neurotransmitter Release in Alzheimer's and Parkinson's Diseases. *Neurodegener. Dis.* **2010**, *7*, 80−83.

(16) Schultz, J.; Uddin, Z.; Singh, G.; Howlader, M. M. Glutamate Sensing in Biofluids: Recent Advances and Research Challenges of Electrochemical Sensors. *Analyst* **2020**, 321.

(17) da Silva Moraes, E. R.; Grisolia, A. B. A.; Oliveira, K. R. M.; Picanço-Diniz, D. L. W.; Crespo-López, M. E.; Maximino, C.; Batista, E. d. J. O.; Herculano, A. M. Determination of Glutamate Uptake by High Performance Liquid Chromatography (Hplc) in Preparations of Retinal Tissue. *J. Chromatogr. B* **2012**, *907*, 1−6.

(18) Bouatra, S.; Aziat, F.; Mandal, R.; Guo, A. C.; Wilson, M. R.; Knox, C.; Bjorndahl, T. C.; Krishnamurthy, R.; Saleem, F.; Liu, P.; et al. The Human Urine Metabolome. *PLoS One* **2013**, *8*, No. e73076.

(19) Burmeister, J. J.; Davis, V. A.; Quintero, J. E.; Pomerleau, F.; Huettl, P.; Gerhardt, G. A. Glutaraldehyde Cross-Linked Glutamate Oxidase Coated Microelectrode Arrays: Selectivity and Resting Levels of Glutamate in the CNS. *ACS Chem. Neurosci.* **2013**, *4*, 721−728.

(20) Burmeister, J. J.; Price, D. A.; Pomerleau, F.; Huettl, P.; Quintero, J. E.; Gerhardt, G. A. Challenges of Simultaneous Measurements of Brain Extracellular Gaba and Glutamate in Vivo Using Enzyme-Coated Microelectrode Arrays. *J. Neurosci. Methods* **2020**, *329*, No. 108435.

(21) Wang, Y.; Mishra, D.; Bergman, J.; Keighron, J. D.; Skibicka, K. P.; Cans, A.-S. Ultrafast Glutamate Biosensor Recordings in Brain Slices Reveal Complex Single Exocytosis Transients. *ACS Chem. Neurosci.* **2019**, *10*, 1744−1752.

(22) Wassum, K. M.; Tolosa, V. M.; Tseng, T. C.; Balleine, B. W.; Monbouquette, H. G.; Maidment, N. T. Transient Extracellular Glutamate Events in the Basolateral Amygdala Track Reward-Seeking Actions. *J. Neurosci.* **2012**, *32*, 2734−2746.

(23) Wang, L.; Li, J.; Feng, M.; Min, L.; Yang, J.; Yu, S.; Zhang, Y.; Hu, X.; Yang, Z. Perovskite-Type Calcium Titanate Nanoparticles as Novel Matrix for Designing Sensitive Electrochemical Biosensing. *Biosens. Bioelectron.* **2017**, *96*, 220−226.

(24) Wang, B.; Gu, S.; Ding, Y.; Chu, Y.; Zhang, Z.; Ba, X.; Zhang, Q.; Li, X. A Novel Route to Prepare Lanio 3 Perovskite-Type Oxide Nanofibers by Electrospinning for Glucose and Hydrogen Peroxide Sensing. *Analyst* **2013**, *138*, 362−367.

(25) Seiyama, T. *Chemical Sensor Technology*; Elsevier, 2013; Vol. 2.

(26) Danbolt, N. C. Glutamate Uptake. *Prog. Neurobiol.* **2001**, *65*, 1−105.

(27) Armbruster, M.; Hanson, E.; Dulla, C. G. Glutamate Clearance Is Locally Modulated by Presynaptic Neuronal Activity in the Cerebral Cortex. *J. Neurosci.* **2016**, *36*, 10404−10415.

(28) Attwell, D.; Laughlin, S. B. An Energy Budget for Signaling in the Grey Matter of the Brain. *J. Cereb. Blood Flow Metab.* **2001**, *21*, 1133−1145.

(29) Pan, S.; Arnold, M. A. Selectivity Enhancement for Glutamate with a Nafion/Glutamate Oxidase Biosensor. *Talanta* **1996**, *43*, 1157−1162.

(30) Hughes, G.; Pemberton, R.; Fielden, P. R.; Hart, J. P. The Design, Development and Application of Electrochemical Glutamate Biosensors. *TrAC, Trends Anal. Chem.* **2016**, *79*, 106−113.

(31) Wassum, K.; Tolosa, V.; Wang, J.; Walker, E.; Monbouquette, H.; Maidment, N. Silicon Wafer-Based Platinum Microelectrode Array Biosensor for near Real-Time Measurement of Glutamate in Vivo. *Sensors* **2008**, *8*, 5023−5036.

(32) Jamal, M.; Worsfold, O.; McCormac, T.; Dempsey, E. A Stable and Selective Electrochemical Biosensor for the Liver Enzyme Alanine Aminotransferase (Alt). *Biosens. Bioelectron.* **2009**, *24*, 2926−2930.

(33) Lowry, J. P.; O'Neill, R. D. Partial Characterization in Vitro of Glucose Oxidase-Modified Poly (Phenylenediamine)-Coated Electrodes for Neurochemical Analysis in Vivo. *Electroanalysis* **1994**, *6*, 369−379.

(34) O'Neill, R. D.; Chang, S.-C.; Lowry, J. P.; McNeil, C. J. Comparisons of Platinum, Gold, Palladium and Glassy Carbon as Electrode Materials in the Design of Biosensors for Glutamate. *Biosens. Bioelectron.* **2004**, *19*, 1521−1528.

(35) Huffman, M. L.; Venton, B. J. Carbon-Fiber Microelectrodes for in Vivo Applications. *Analyst* **2009**, *134*, 18−24.

(36) Ammam, M.; Fransaer, J. Highly Sensitive and Selective Glutamate Microbiosensor Based on Cast Polyurethane/Ac-Electro-phoresis Deposited Multiwalled Carbon Nanotubes and Then

Glutamate Oxidase/Electrosynthesized Polypyrrole/Pt Electrode. *Biosens. Bioelectron.* **2010**, *25*, 1597−1602.

(37) Hughes, G. *The Design, Development and Application of Novel, Screen-Printed Amperometric Glutamate Biosensors*; University of the West of England, 2015.

(38) Rahman, M. A.; Kwon, N.-H.; Won, M.-S.; Choe, E. S.; Shim, Y.-B. Functionalized Conducting Polymer as an Enzyme-Immobilizing Substrate: An Amperometric Glutamate Microbiosensor for in Vivo Measurements. *Anal. Chem.* **2005**, *77*, 4854−4860.

(39) Özel, R. E.; Ispas, C.; Ganesana, M.; Leiter, J.; Andreescu, S. Glutamate Oxidase Biosensor Based on Mixed Ceria and Titania Nanoparticles for the Detection of Glutamate in Hypoxic Environments. *Biosens. Bioelectron.* **2014**, *52*, 397−402.

(40) Dalkıran, B.; Erden, P. E.; Kılıç, E. Graphene and Tricobalt Tetraoxide Nanoparticles Based Biosensor for Electrochemical Glutamate Sensing. *Artif. Cells, Nanomed., Biotechnol.* **2017**, *45*, 340−348.

(41) Dai, H.; Zhong, Y.; Wu, X.; Hu, R.; Wang, L.; Zhang, Y.; Fan, G.; Hu, X.; Li, J.; Yang, Z. Synthesis of Perovskite-Type Srtio3 Nanoparticles for Sensitive Electrochemical Biosensing Applications. *J. Electroanal. Chem.* **2018**, *810*, 95−99.

(42) Rutherford, E. C.; Pomerleau, F.; Huettl, P.; Strömberg, I.; Gerhardt, G. A. Chronic Second-by-Second Measures of L-Glutamate in the Central Nervous System of Freely Moving Rats. *J. Neurochem.* **2007**, *102*, 712−722.

(43) Mattinson, C. E.; Burmeister, J. J.; Quintero, J. E.; Pomerleau, F.; Huettl, P.; Gerhardt, G. A. Tonic and Phasic Release of Glutamate and Acetylcholine Neurotransmission in Sub-Regions of the Rat Prefrontal Cortex Using Enzyme-Based Microelectrode Arrays. *J. Neurosci. Methods* **2011**, *202*, 199−208.

(44) Clay, M.; Monbouquette, H. G. A Detailed Model of Electroenzymatic Glutamate Biosensors to Aid in Sensor Optimization and in Applications in Vivo. *ACS Chem. Neurosci.* **2018**, *9*, 241−251.

(45) Shi, J.; Zhou, Y.; Ramanathan, S. Colossal Resistance Switching and Band Gap Modulation in a Perovskite Nickelate by Electron Doping. *Nat. Commun.* **2014**, *5*, No. 4860.

(46) Oh, C.; Jo, M.; Son, J. All-Solid-State Synaptic Transistors with High-Temperature Stability Using Proton Pump Gating of Strongly Correlated Materials. *ACS Appl. Mater. Interfaces* **2019**, *11*, 15733−15740.

(47) Ganesana, M.; Trikantzopoulos, E.; Maniar, Y.; Lee, S. T.; Venton, B. J. Development of a Novel Micro Biosensor for in Vivo Monitoring of Glutamate Release in the Brain. *Biosens. Bioelectron.* **2019**, *130*, 103−109.

(48) Miele, M.; Fillenz, M. In Vivo Determination of Extracellular Brain Ascorbate. *J. Neurosci. Methods* **1996**, *70*, 15−19.

(49) Weltin, A.; Kieninger, J.; Enderle, B.; Gellner, A.-K.; Fritsch, B.; Urban, G. A. Polymer-Based, Flexible Glutamate and Lactate Microsensors for in Vivo Applications. *Biosens. Bioelectron.* **2014**, *61*, 192−199.

(50) Burmeister, J. J.; Gerhardt, G. A. Self-Referencing Ceramic-Based Multisite Microelectrodes for the Detection and Elimination of Interferences from the Measurement of L-Glutamate and Other Analytes. *Anal. Chem.* **2001**, *73*, 1037−1042.

(51) Stephens, M. L.; Quintero, J. E.; Pomerleau, F.; Huettl, P.; Gerhardt, G. A. Age-Related Changes in Glutamate Release in the Ca3 and Dentate Gyrus of the Rat Hippocampus. *Neurobiol. Aging* **2011**, *32*, 811−820.

(52) Batra, B.; Pundir, C. An Amperometric Glutamate Biosensor Based on Immobilization of Glutamate Oxidase onto Carboxylated Multiwalled Carbon Nanotubes/Gold Nanoparticles/Chitosan Composite Film Modified Au Electrode. *Biosens. Bioelectron.* **2013**, *47*, 496−501.

(53) Hamdi, N.; Wang, J.; Walker, E.; Maidment, N. T.; Monbouquette, H. G. An Electroenzymatic L-Glutamate Microbiosensor Selective against Dopamine. *J. Electroanal. Chem.* **2006**, *591*, 33−40.

(54) Sirca, D.; Vardeu, A.; Pinna, M.; Diana, M.; Enrico, P. A Robust, State-of-the-Art Amperometric Microbiosensor for Glutamate Detection. *Biosens. Bioelectron.* **2014**, *61*, 526−531.

(55) Maity, D.; Kumar, R. R. Highly Sensitive Amperometric Detection of Glutamate by Glutamic Oxidase Immobilized Pt Nanoparticle Decorated Multiwalled Carbon Nanotubes (Mwcnts)/Polypyrrole Composite. *Biosens. Bioelectron.* **2019**, *130*, 307−314.

(56) Govindarajan, S.; McNeil, C. J.; Lowry, J. P.; McMahon, C. P.; O'Neill, R. D. Highly Selective and Stable Microdisc Biosensors for L-Glutamate Monitoring. *Sens. Actuators, B* **2013**, *178*, 606−614.

(57) Jamal, M.; Xu, J.; Razeeb, K. M. Disposable Biosensor Based on Immobilisation of Glutamate Oxidase on Pt Nanoparticles Modified Au Nanowire Array Electrode. *Biosens. Bioelectron.* **2010**, *26*, 1420−1424.

(58) Kwong, A. W.; Gründig, B.; Hu, J.; Renneberg, R. Comparative Study of Hydrogel-Immobilized L-Glutamate Oxidases for a Novel Thick-Film Biosensor and Its Application in Food Samples. *Biotechnol. Lett.* **2000**, *22*, 267−272.

(59) Moussawi, K.; Riegel, A.; Nair, S.; Kalivas, P. W. Extracellular Glutamate: Functional Compartments Operate in Different Concentration Ranges. *Front. Syst. Neurosci.* **2011**, *5*, No. 94.

(60) Clay, M.; Monbouquette, H. G. A Detailed Model of Electroenzymatic Glutamate Biosensors to Aid in Sensor Optimization and in Applications in Vivo. *ACS Chem. Neurosci.* **2018**, *9*, 241−251.

(61) Kirkwood, A.; Dudek, S. M.; Gold, J. T.; Aizenman, C. D.; Bear, M. F. Common Forms of Synaptic Plasticity in the Hippocampus and Neocortex in Vitro. *Science* **1993**, *260*, 1518−1521.

(62) Lein, E. S.; Hawrylycz, M. J.; Ao, N.; Ayres, M.; Bensinger, A.; Bernard, A.; Boe, A. F.; Boguski, M. S.; Brockway, K. S.; Byrnes, E. J. Genome-Wide Atlas of Gene Expression in the Adult Mouse Brain. *Nature* **2007**, *445*, 168.

(63) Kissinger, S. T.; Pak, A.; Tang, Y.; Masmanidis, S. C.; Chubykin, A. A. Oscillatory Encoding of Visual Stimulus Familiarity. *J. Neurosci.* **2018**, *38*, 6223−6240.

(64) Nguyen, T. N. H.; Nolan, J. K.; Park, H.; Lam, S.; Fattah, M.; Page, J. C.; Joe, H.-E.; Jun, M. B. G.; Lee, H.; Kim, S. J.; Shi, R.; Lee, H. Facile Fabrication of Flexible Glutamate Biosensor Using Direct Writing of Platinum Nanoparticle-Based Nanocomposite Ink. *Biosens. Bioelectron.* **2019**, *131*, 257−266.

(65) Wu, Q.; Kolb, I.; Callahan, B. M.; Su, Z.; Stoy, W.; Kodandaramaiah, S. B.; Neve, R.; Zeng, H.; Boyden, E. S.; Forest, C. R.; Chubykin, A. A. Integration of Autopatching with Automated Pipette and Cell Detection in Vitro. *J. Neurophysiol.* **2016**, *116*, 1564−1578.

(66) Kissinger, S. T.; Pak, A.; Tang, Y.; Masmanidis, S. C.; Chubykin, A. A. Oscillatory Encoding of Visual Stimulus Familiarity. *J. Neurosci.* **2018**, *38*, 6223−6240.

(67) Pachitariu, M.; Steinmetz, N. A.; Kadir, S. N.; Carandini, M.; Harris, K. D. In *Fast and Accurate Spike Sorting of High-Channel Count Probes with Kilosort*, Advances in Neural Information Processing Systems, 2016; pp 4448−4456.

(68) Rossant, C.; Kadir, S. N.; Goodman, D. F.; Schulman, J.; Hunter, M. L.; Saleem, A. B.; Grosmark, A.; Belluscio, M.; Denfield, G. H.; Ecker, A. S.; et al. Spike Sorting for Large, Dense Electrode Arrays. *Nat. Neurosci.* **2016**, *19*, 634.